Princeton Plasma Physics Laboratory

PPPL- 5018

PPPL- 5018

Laboratory Study Of Magnetic Reconnecion With A Density Asymmetry Across The Current Sheet

Jongsoo Yoo, et. al.

APRIL, 2014

PPPL PRINCETON PLASMA PHYSICS LABORATORY

Prepared for the U.S. Department of Energy under Contract DE-AC02-09CH11466.

Princeton Plasma Physics Laboratory
Report Disclaimers

Full Legal Disclaimer

Trademark Disclaimer

PPPL Report Availability

Princeton Plasma Physics Laboratory:

http://www.pppl.gov/techreports.cfm

Office of Scientific and Technical Information (OSTI):

http://www.osti.gov/bridge

Related Links:

U.S. Department of Energy

Office of Scientific and Technical Information

Fusion Links

Laboratory Study of Magnetic Reconnection with a Density Asymmetry across the Current Sheet

Jongsoo Yoo,* Masaaki Yamada, Hantao Ji, Clayton E. Myers, and Jonathan Jara-Almonte

Center for Magnetic Self-organization in Laboratory and Astrophysical Plasmas,

Princeton Plasma Physics Laboratory,

Princeton, New Jersey 08543, USA.

Li-Jen Chen

Space Science Center, University of New Hampshire,

Durham, New Hampshire 03824, USA

(Dated: April 13, 2014)

Abstract

The effects of an upstream density asymmetry on magnetic reconnection are studied systematically in a laboratory plasma. Despite a significant upstream density asymmetry of up to 10, the reconnecting magnetic field profile is not significantly changed. On the other hand, the out-of-plane magnetic field profile is considerably modified; it is almost bipolar in structure with the density asymmetry, as compared to the quadrupolar structure in the symmetric configuration. The in-plane ion flow pattern and the electrostatic potential profile are also affected by the density asymmetry. Strong bulk electron heating is observed near the low-density-side separatrix together with electromagnetic fluctuations in the lower hybrid frequency range. The dependence of the ion outflow and reconnection electric field on the density asymmetry is measured and compared with theoretical expectations.

PACS numbers: 52.35.Vd, 52.30.-q

Magnetic reconnection is a fundamental process in magnetized plasmas which converts magnetic energy to particle energy. Magnetic reconnection plays a key role in explosive phenomena in the universe such as geomagnetic storms, solar eruptions, and stellar flares [1–3]. Although the majority of theoretical and computational studies on magnetic reconnection assume that the plasma parameters on both sides of the current sheet are similar, magnetic reconnection often occurs with considerable asymmetries in upstream plasma parameters such as the plasma density and magnetic field strength. For example, at the subsolar magnetopause, where the solar wind plasma interacts with the magnetospheric plasma, reconnection is mostly asymmetric with a large upstream density ratio of 10–100 and a magnetic field strength ratio of 2–3 [4, 5]. This so-called asymmetric reconnection is of importance due to its generality and applicability to real physical situations in both astrophysical plasmas [5] and magnetically-confined laboratory plasmas [6, 7].

Features of asymmetric reconnection have been observed in space [8, 9] and numerical simulations [10–12]. In particular, the out-of-plane quadrupole magnetic field (QF) and the in-plane bipolar electric field, which are two signatures of collisionless reconnection, become almost bipolar and unipolar, respectively. Moreover, strong density gradients forms near the low-density-side separatrix where strong electric field fluctuations are frequently observed [13, 14]. The upstream density asymmetry also impacts the ion flow pattern by shifting the ion inflow stagnation point to the low-density side [10, 15].

The effects of asymmetrical upstream parameters on the reconnection rate and other exhaust-region properties, such as the density and outflow velocity, have been studied by a Sweet-Parker-type analysis [15]. Various 2-D MHD simulations were performed to understand how the reconnection rate is determined during asymmetric reconnection [15–17]. Recently, the general scaling for asymmetric reconnection [15] has been tested in both two-fluid simulations [18, 19] and particle-in-cell simulations [12].

Although there has been progress in understanding asymmetric reconnection, systematic experimental studies play an essential role in cross-validating observations in space and numerical simulations. In this letter, the first quantitative analysis on asymmetric reconnection in a laboratory plasma is reported. Plasmas with a significant upstream density ratio of up to 10 are created and compared with a plasma with an upstream density ratio of about 1.2. Key features of asymmetric reconnection, such as the modified QF and in-plane electrostatic potential, are experimentally verified. An asymmetric ion flow profile shows that the ion

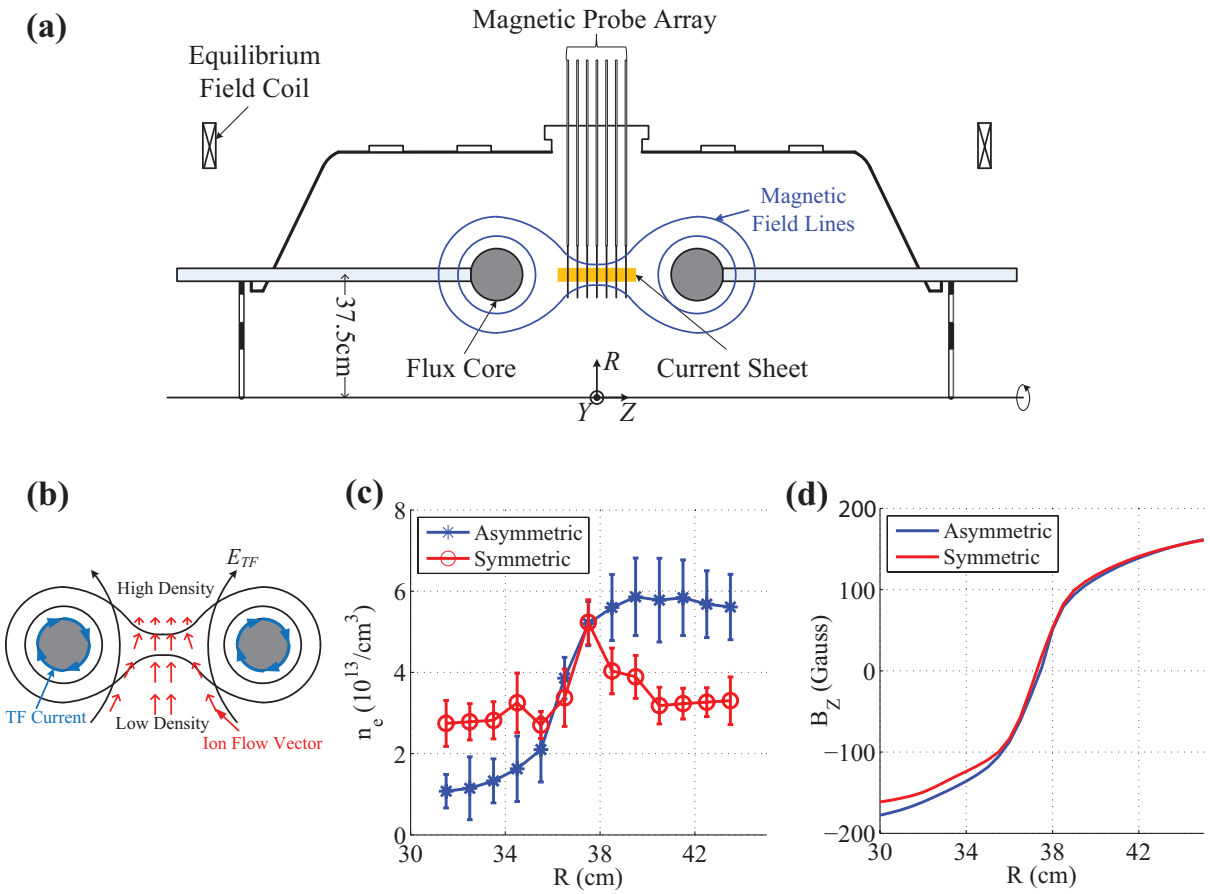

FIG. 1. (color online)(a) A cross section of MRX. The flux core contains both the PF coil for driving magnetic reconnection and the TF coil for creating the plasma. Magnetic probes are inserted to monitor the evolution of the 2-D magnetic geometry. (b) Schematic view of the ion dynamics during the plasma formation period. The blue arrows indicate the direction of the TF coil current. The red arrows stand for the ion flow vectors. (c) Radial electron density profiles at $Z = 0$ for both asymmetric and symmetric cases early in the quasi-steady period. (d) Radial profiles of the reconnecting magnetic field component (B_Z) at $Z = 0$ early in the quasi-steady period.

stagnation point is shifted to the low-density side. A strong bulk electron heating is observed near the low-density-side separatrix where electromagnetic fluctuations in the lower hybrid frequency range are observed. Finally, both the ion outflow velocity and reconnection electric field are measured and compared with the general scaling laws in Ref. [15].

These experiments were performed at the Magnetic Reconnection Experiment (MRX) facility [20]. Figure 1-(a) shows a cross section of the MRX device in the R–Z plane. The

two gray circles are "flux cores" that each contain two independent coils: a poloidal field (PF) coil and a toroidal field (TF) coil. The PF coils produce the X-line magnetic field geometry, and reconnection is driven by decreasing the PF coil current [20]. The TF coils inductively create the plasma around the flux cores. No significant guide field exists during the quasi-steady reconnection period over which the reconnection rate is relatively constant. The current sheet is elongated along the Z direction during the quasi-steady period, such that the coordinate system in this letter is the following: R is the normal to the current sheet; Z is the outflow direction; Y is the symmetric, out-of-plane direction.

As illustrated in Fig. 1-(b), the upstream density asymmetry is generated during the plasma formation period due to the inductive electric field, E_{TF}, from the increasing TF coil current. For this experimental campaign, the direction of E_{TF} at the center of the X-line is radially outward during the plasma formation. Then, ions are transported outward along E_{TF}, generating a radial density asymmetry. This radial density asymmetry remains over the quasi-steady reconnection period, and the degree of asymmetry can be controlled by changing the TF current waveform and using different gas species. For example, we use helium to create an asymmetric plasma, and deuterium to create a relatively symmetric plasma. In addition, the helium fill pressure is varied for further control of the upstream density ratio up to 10.

The main diagnostic for this study is a 2-D magnetic probe array which consists of 250 small pick-up coils. The probe array measures the evolution of all three components of the magnetic field with a maximum radial (R) resolution of 0.6 cm and an axial (Z) spacing of 3 cm. The electron density (n_e) and temperature (T_e) are measured by triple Langmuir probes. The plasma potential (Φ_p) is obtained by measuring floating potential and electron temperature profiles [21]. The ion flow vectors ($\mathbf{V}_i$) are measured by Mach probes which were previously calibrated by spectroscopic data [21]. A fluctuation probe is used to measure all three components of magnetic fluctuations and the out-of-plane (Y) component of electrostatic fluctuations in the floating potential. Extensive R-Z scans of Langmuir probes and Mach probes are conducted to obtain 2-D profiles of n_e, T_e, Φ_p, and $\mathbf{V}_i$ for both asymmetric (4.5 mT helium discharges) and symmetric (4 mT deuterium discharges) cases. Reproducibility of both the data from the 2-D magnetic probe array and a reference Langmuir probe is examined to find similar discharges.

Figure 1-(c) shows clear differences in the radial density profile at $Z = 0$ between the

asymmetric and symmetric case early in the quasi-steady period. For the asymmetric case, the outboard side ($R > 37.5$ cm) has about 6 times larger density than the inboard side ($R < 37.5$ cm). The main transition from the low to high density is shifted to the low-density side ($R < 37.5$ cm). The measured 2-D density profile (not shown) shows that strong density gradients occur in the vicinity of the low-density-side separatrix throughout the downstream region, which is consistent with numerical simulations [10–12]. For the symmetric case, the upstream density is very similar and the density peaks at the center of the current sheet ($R = 37.5$ cm).

The reconnecting magnetic field (B_Z) profiles at $Z = 0$ are remarkably similar for both cases, as shown in Fig. 1-(d). Despite the large density asymmetry, the low-density side has only about 15% larger B_Z magnitude than the high-density side. The magnetic pressure difference between the two sides of the current sheet is only about 15 Pa, which is not enough to enforce pressure balance across the current sheet if the electron and ion temperature on each side are similar. Thus, electron and ion temperature are expected to be higher on the low-density side. The T_e profile is indeed asymmetric (see Fig. 4-(a)) with higher temperatures on the low-density side, but the difference is not enough to satisfy pressure balance. This indicates that the ion temperature on the low-density side should be also higher. Due to the lack of ion temperature measurements with a high radial resolution, however, this argument has not been confirmed.

While the upstream density asymmetry does not affect the in-plane magnetic geometry, it significantly modifies the QF profile, as shown in Fig. 2-(a) and (b). The black lines indicate contours of the poloidal magnetic flux, $\Psi \equiv \int_0^R 2\pi R' B_Z dR'$, which represent the magnetic field lines in the R-Z plane. There is no noticeable difference in the magnetic geometry between the two cases. On the other hand, the QF profile for the asymmetric case is significantly different from that of the symmetric case; the magnitude of the QF is about 6 times larger on the high-density side than on the low-density side.

This asymmetric QF profile can be explained by the Hall term in the generalized Ohm's law. The reconnection electric field (E_{rec}) is relatively uniform on both sides during the quasi-steady reconnection period, and it is balanced by the $\mathbf{J} \times \mathbf{B}$ Hall term in the upstream region [22]. Thus, we have

$$E_{rec} \approx -\frac{J_1 B_1}{e n_1} \approx -\frac{J_2 B_2}{e n_2}, \tag{1}$$

where subscript 1 indicates upstream quantities on the high-density side, while the subscript

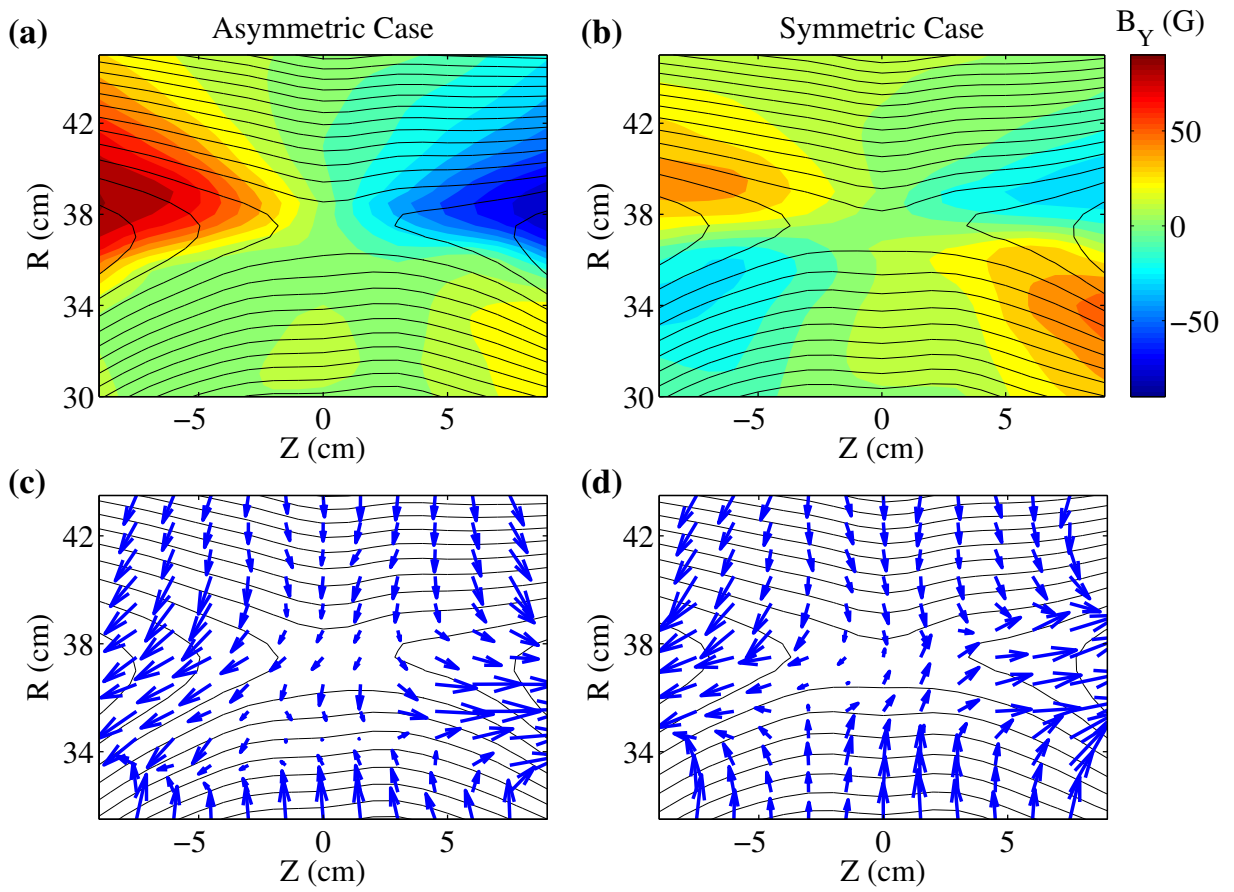

FIG. 2. (color) 2-D profiles of the out-of-plane magnetic field (B_Y) with contours of the poloidal flux for asymmetric (a) and symmetric (b) cases. Compared to the symmetric case, the quadrupole magnetic field component is enhanced on the high-density side ($R > 37.5$ cm) and suppressed on the low-density side ($R < 37.5$ cm). Black lines indicate contours of the poloidal magnetic flux which represent magnetic field lines. In-plane ion flow vector profiles for asymmetric (c) and symmetric (d) cases. For the asymmetric case, the ion inflow stagnation point is shifted to the low-density side. The upstream density ratio (n_1/n_2) for the asymmetric case is about 6, while it is about 1.2 for the symmetric case.

2 means those on the low-density side. From this equation, the Hall current of the high-density side, $J_1 \approx (n_1 B_2)/(n_2 B_1) J_2 \approx (n_1/n_2) J_2$ is larger by about the upstream density ratio. Since the QF is generated by the Hall current, the high-density side has a larger magnitude of the QF.

The in-plane ion flow pattern is affected by the upstream density asymmetry as shown

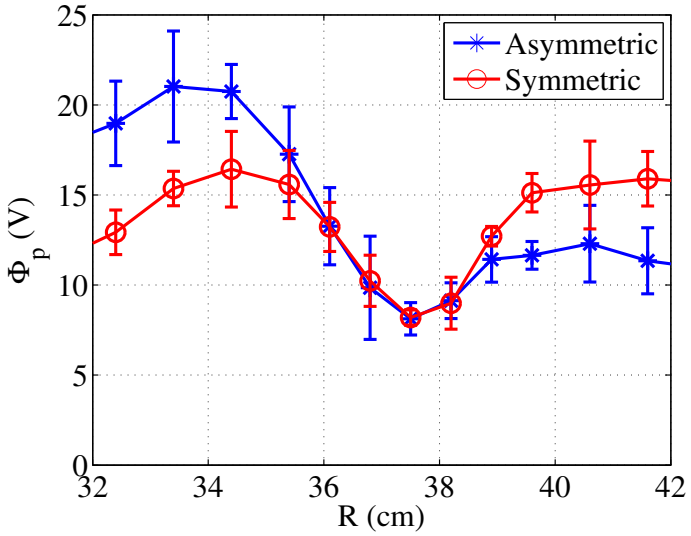

FIG. 3. (color online) Radial plasma potential profiles at $Z = 0$ for asymmetric (blue) and symmetric (red) cases. With the density asymmetry, the potential profile becomes asymmetric with a larger well depth on the low-density side.

in Fig. 2-(c) and (d). For the asymmetric case, the inflow ion stagnation point is shifted to $R \sim 34.5$ cm, while the X-point is at 37.5 cm. For the symmetric case, the stagnation point at $Z = 0$ is almost at the same location as the X-point. This shift of stagnation point is due to the imbalance of the incoming mass flux [15] and is observed in numerical simulations [10]. It is worth noting that the ion outflow is also asymmetric, especially on the left side ($Z = 7.5$ cm); the ion outflow is stronger on the low-density side that has a larger upstream Alfvén velocity [17].

The upstream density asymmetry also modifies the in-plane electrostatic potential profile, which is another signature of collisionless reconnection. The in-plane electrostatic potential has a "well" structure along the direction normal to the current sheet [21, 23–25]. Figure 3 shows radial potential profiles at $Z = 0$ for both asymmetric and symmetric cases. The depth of the potential well on the low-density side is about 3–4 times larger than the that on the low-density side. For the symmetric case, the potential profile is balanced with a well depth of about 9 V. This modified potential profile is expected since the depth of the potential well scales as B^2/n_e [26].

Figure 4-(a) shows the measured 2-D electron temperature profile. Electrons are strongly

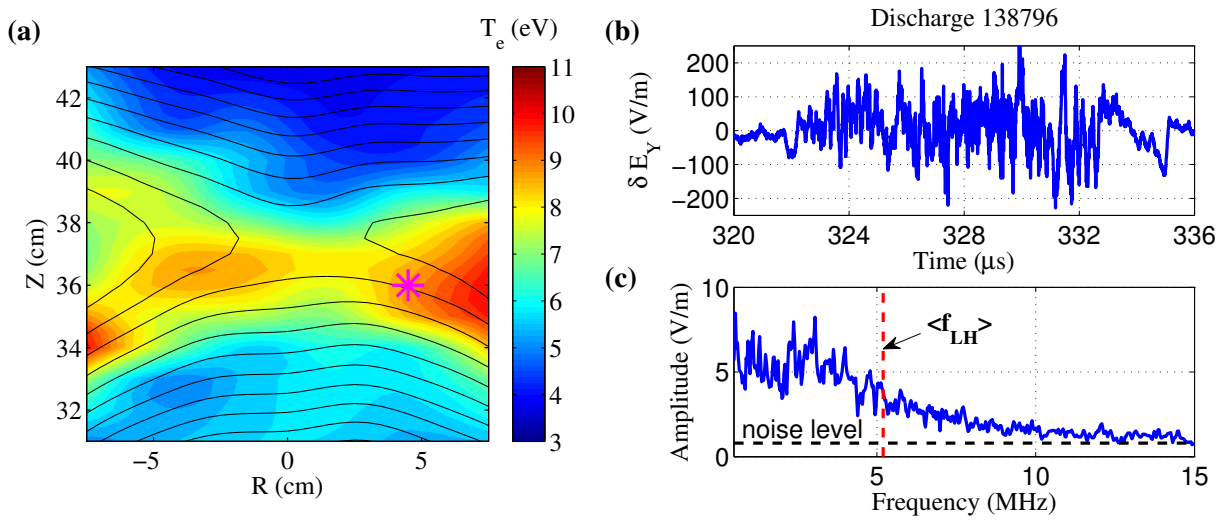

FIG. 4. (color online) (a) 2-D electron temperature profile for the asymmetric case. Strong bulk electron heating exists near the low-density-side separatrix. The magenta asterisk indicates the measurement location of high-frequency fluctuations. (b) Time trace of typical fluctuations in E_Y (Discharge 138796). (c) Fourier spectrum of δE_Y averaged over 12 discharges.

heated near the low-density-side separatrix where fluctuations in both E_Y and $\mathbf{B}$ are observed. Figure 4-(b) shows a time trace of fluctuations in the out-of-plane electric field (δE_Y). The trace of fluctuations in the magnetic field is similar, and typical amplitudes of δE_Y and δB are 100 V/m and 7 Gauss, respectively. The averaged Fourier spectrum in Fig. 4-(c) shows that these fluctuations are broad-band and that the energy is mostly concentrated below the lower-hybrid frequency, f_{LH}. These characteristics are consistent with LHDI driven turbulence [13, 14, 27, 28]. The free energy source of LHDI is the strong density gradient in the vicinity of the low-density-side separatrix [13]. This LHDI driven turbulence may contribute to the observed bulk electron heating [28]. However, the effective electron heating by the parallel electric field can also play a role [29]. The parallel electric field in the asymmetric configuration exists only on the low-density side [29]. The measured 2-D profile supports the existence of the parallel electric field, since the upstream temperature on the low-density side ($\sim$ 6 eV) is higher than the high-density side ($\sim$ 4 eV).

Finally, the general scaling for the ion outflow and reconnection electric field given by Ref. [15] is tested by systematically varying the upstream density ratio (n_1/n_2). Plasmas with different $n_1 = (1.3\text{–}10) \times 10^{13}$ /cm^3 and relatively constant $n_2 \sim 1 \times 10^{13}$ /cm^3 are

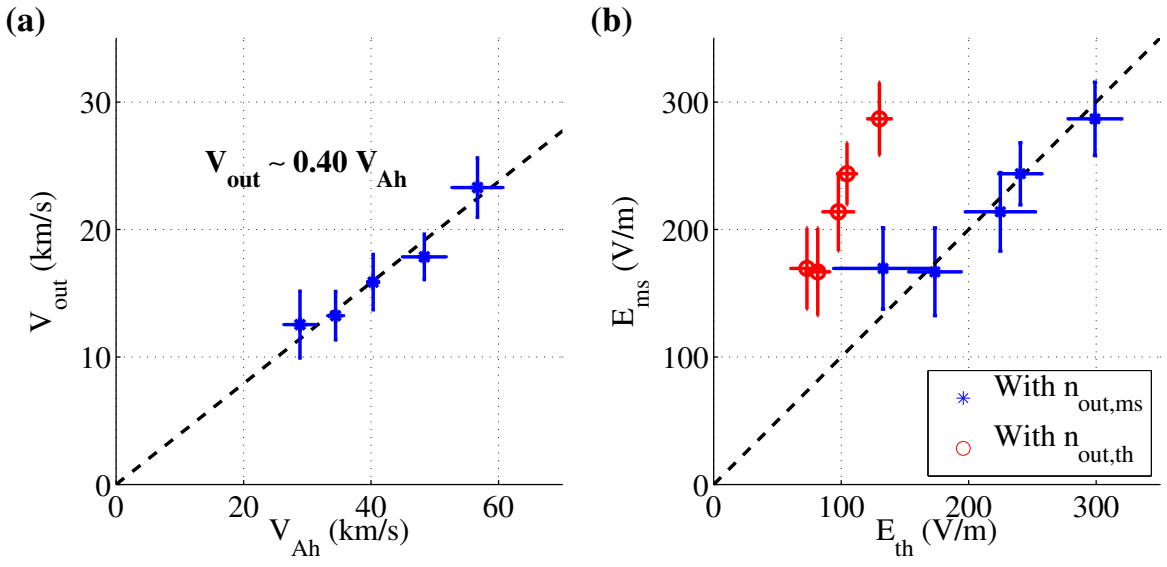

FIG. 5. (color online) (a) Measured ion outflow velocity compared to the hybrid Alfvén velocity. The measured values are about 40% of theoretically predicted values. The black dashed line indicates a linear fit. (b) The measured reconnection electric field versus E_{th} in Eqn. 3. Values of E_{ms} agree with those of E_{th} when the measured outflow density, $n_{out,ms}$ (blue asterisks) is used as n_{out} instead of the theoretical estimate, $n_{out,th}$ (red circles).

created. The ion outflow is measured at $\sim 2d_i$ away from the X-point where $d_i \equiv c/\omega_{pi}$ is the ion skin depth based on n_2. As shown in Fig. 5-(a), the measured outflow velocity V_{out} is only 40% of the theoretically predicted outflow velocity V_{Ah}. Here, V_{Ah} is a hybrid Alfvén velocity defined as [15]

$$m_i V_{Ah}^2 = \frac{S_1 + S_2}{n_1 V_1 + n_2 V_2} = \frac{B_1 B_2 (B_1 + B_2)}{\mu_0 (n_1 B_2 + n_2 B_1)}, \tag{2}$$

where S_1 and S_2 are the incoming Poynting fluxes and V_1 and V_2 are the inflow speeds. Since $m_i V_{Ah}^2$ is the ratio of incoming Poynting fluxes and particle fluxes, it physically represents the available magnetic energy per an ion-electron pair [30]. Therefore, for the plasma to have the outflow speed of V_{Ah}, about one half of the available magnetic energy would have to be converted to the ion flow energy. However, the energy inventory during magnetic reconnection generally favors increasing the ion thermal energy rather than flow energy [17, 31–33]. In MRX, there is another possible reason for the low outflow velocity, which is the high downstream pressure due to the existence of the flux cores [21, 34].

The measured reconnection electric field (E_{ms}) is also compared to the theoretical prediction (E_{th}), which is given by [15]

$$E_{th} = \frac{2\delta}{L} V_{out} \frac{n_{out} B_1 B_2}{n_1 B_2 + n_2 B_1}, \tag{3}$$

where δ and L are the half width and length of the diffusion region, respectively, and n_{out} is the density at the outflow region. By arguing n_{out} is the effective density of a newly reconnected flux tube, the theoretical estimate of n_{out} is given by [15]

$$n_{out,th} = \frac{B_1 n_2 + B_2 n_1}{B_1 + B_2}. \tag{4}$$

However, the measured density at the outflow region, $n_{out,ms}$ is about $2n_{out,th}$. As shown in Fig. 5-(b), E_{ms} agrees with E_{th} only if we use the measured outflow density as n_{out} in Eqn. 3.

In summary, we studied reconnection with a significant upstream density asymmetry in a laboratory plasma. The observed features of asymmetric reconnection agree with the previous observations in space and numerical simulations. The upstream density asymmetry modifies the in-plane ion flow pattern as well as the Hall fields - quadrupole out-of-plane magnetic field and in-plane electrostatic field. However, the in-plane magnetic field geometry is barely affected. Strong bulk electron heating is observed near the low-density-side separatrix together with electromagnetic fluctuations driven by LHDI. Mechanisms for the electron heating require further research. The ion outflow and reconnection electric field are measured and compared with theoretical predictions. The ion outflow speed is about 40% of the hybrid Alfvén velocity and the reconnection electric field agrees with the scaling, provided that the measured plasma density in the exhaust region is used instead of the theoretically predicted value. In the future, direct comparisons between laboratory data and spacecraft data at the subsolar magnetopause will be attempted for more understanding of particle energization during asymmetric reconnection.

This work is supported by DOE, NSF, and NASA. The authors thank J, Drake, V. Roytershteyn, and W. Daughton for valuable discussions, and R. Cutler for technical support.

* jyoo@pppl.gov

[1] E. Priest and T. Forbes, *Magnetic reconnection - MHD theory and applications* (Cambridge University Press, New York, USA, 2000).

[2] E. G. Zweibel and M. Yamada, Annu. Rev. Astron. Astr. **47**, 291 (2009).

[3] M. Yamada, R. Kulsrud, and H. Ji, Rev. Mod. Phys. **82**, 603 (2010).

[4] F. S. Mozer and A. Retinò, J. Geophys. Res. **112**, A10206 (2007).

[5] F. S. Mozer and P. L. Pritchett, Space Sci. Rev. **158**, 119 (2011).

[6] L. Zakharov, B. Rogers, and S. Migliuolo, Physics of Fluids B: Plasma Physics (1989-1993) **5**, 2498 (1993).

[7] M. T. Beidler and P. A. Cassak, Phys. Rev. Lett. **107**, 255002 (2011).

[8] F. S. Mozer, V. Angelopoulos, J. Bonnell, K. H. Glassmeier, and J. P. McFadden, Geophys. Res. Lett. **35**, L17S04 (2008).

[9] F. S. Mozer, P. L. Pritchett, J. Bonnell, D. Sundkvist, and M. T. Chang, J. Geophys. Res. **113**, A00C03 (2008).

[10] P. L. Pritchett, J. Geophys. Res. **113**, A06210 (2008).

[11] K. G. Tanaka, A. Retinò, Y. Asano, M. Fujimoto, I. Shinohara, A. Vaivads, Y. Khotyaintsev, M. André, M. B. Bavassano-Cattaneo, S. C. Buchert, and C. J. Owen, Ann. Geophys. **26**, 2471 (2008).

[12] K. Malakit, M. A. Shay, P. A. Cassak, and C. Bard, J. Geophys. Res. **115**, A10223 (2010).

[13] P. L. Pritchett, F. S. Mozer, and M. Wilber, J. Geophys. Res. **117**, A06212 (2012).

[14] V. Roytershteyn, W. Daughton, H. Karimabadi, and F. S. Mozer, Phys. Rev. Lett. **108**, 185001 (2012).

[15] P. A. Cassak and M. A. Shay, Phys. Plasmas **14**, 102114 (2007).

[16] J. E. Borovsky and M. Hesse, Phys. Plasmas **14**, 102309 (2007).

[17] J. Birn, J. E. Borovsky, and M. Hesse, Phys. Plasmas **15**, 032101 (2008).

[18] P. A. Cassak and M. A. Shay, Geophys. Res. Lett. **35**, L19102 (2008).

[19] P. A. Cassak and M. A. Shay, Phys. Plasmas **16**, 055704 (2009).

[20] M. Yamada, H. Ji, S. Hsu, T. Carter, R. Kulsrud, N. Bretz, F. Jobes, Y. Ono, and F. Perkins, Phys. Plasmas **4**, 1936 (1997).

[21] J. Yoo, M. Yamada, H. Ji, and C. E. Myers, Phys. Rev. Lett. **110**, 215007 (2013).

[22] Y. Ren, M. Yamada, H. Ji, S. Dorfman, S. P. Gerhardt, and R. Kulsrud, Phys. Plasmas **15**, 082113 (2008).

[23] J. R. Wygant, C. A. Carttell, R. Lysak, Y. Song, J. Dombeck, J. McFadden, F. S. Mozer, C. W. Carlson, G. Parks, E. A. Lucek, A. Balogh, M. Andre, H. Reme, M. Hesse, and C. Mouikis, J. Geophys. Res. **110**, A09206 (2005).

[24] H. Karimabadi, W. Daughton, and J. Scudder, Geophys. Res. Lett. **34**, L13104 (2007).

[25] L.-J. Chen, N. Bessho, B. Lefebvre, H. Vaith, A. Fazakerley, A. Bhattacharjee, P. A. Puhl-Quinn, A. Runov, Y. Khotyaintsev, A. Vaivads, E. Georgescu, and R. Torbert, J. Geophys. Res. **113**, A12213 (2008).

[26] J. Yoo, M. Yamada, H. Ji, J. Jara-Almonte, and C. E. Myers, "Bulk ion acceleration and particle heating during magnetic reconnection in a laboratory plasma," To be published in Phys. Plasmas.

[27] T. A. Carter, H. Ji, F. Trintchouk, M. Yamada, and R. M. Kulsrud, Phys. Rev. Lett. **88**, 015001 (2001).

[28] C. Tang, X.and Cattell, J. Dombeck, L. Dai, L. B. Wilson, A. Breneman, and A. Hupach, Geophys. Res. Lett. **40**, 2884 (2013).

[29] J. Egedal, A. Le, P. L. Pritchett, and W. Daughton, Phys. Plasmas **18**, 102901 (2011).

[30] T. D. Phan, M. A. Shay, J. T. Gosling, M. Fujimoto, J. F. Drake, G. Paschmann, M. Oieroset, J. P. Eastwood, and V. Angelopoulos, Geophys. Res. Lett. **40**, 4475 (2013).

[31] N. Aunai, G. Belmont, and R. Smets, Phys. Plasmas **18**, 122901 (2011).

[32] J. P. Eastwood, T. D. Phan, J. F. Drake, M. A. Shay, A. L. Borg, B. Lavraud, and M. G. G. T. Taylor, Phys. Rev. Lett. **110**, 225001 (2013).

[33] M. Yamada, J. Yoo, J. Jara-Almonte, H. Ji, R. M. Kulsrud, and C. E. Myers, "Energy conversion in the magnetic reconnection layer of a laboratory plasma," To be published.

[34] H. Ji, M. Yamada, S. Hsu, and R. Kulsrud, Phys. Rev. Lett. **80**, 3256 (1998).

The Princeton Plasma Physics Laboratory is operated
by Princeton University under contract
with the U.S. Department of Energy.

Information Services
Princeton Plasma Physics Laboratory
P.O. Box 451
Princeton, NJ 08543

Phone: 609-243-2245
Fax: 609-243-2751
e-mail: pppl_info@pppl.gov
Internet Address: http://www.pppl.gov